

Tennessee State University

Digital Scholarship @ Tennessee State University

Agricultural and Environmental Sciences
Faculty Research

Department of Agricultural and Environmental
Sciences

1-2022

Examining the Integration of Landsat Operational Land Imager with Sentinel-1 and Vegetation Indices in Mapping Southern Yellow Pines (Loblolly, Shortleaf, and Virginia Pines)

Clement E. Akumu

Eze O. Amadi

Follow this and additional works at: <https://digitalscholarship.tnstate.edu/agricultural-and-environmental-sciences-faculty>

 Part of the Forest Sciences Commons

Examining the Integration of Landsat Operational Land Imager with Sentinel-1 and Vegetation Indices in Mapping Southern Yellow Pines (Loblolly, Shortleaf, and Virginia Pines)

Clement E. Akumu and Eze O. Amadi

Abstract

The mapping of southern yellow pines (loblolly, shortleaf, and Virginia pines) is important to supporting forest inventory and the management of forest resources. The overall aim of this study was to examine the integration of Landsat Operational Land Imager (OLI) optical data with Sentinel-1 microwave C-band satellite data and vegetation indices in mapping the canopy cover of southern yellow pines. Specifically, this study assessed the overall mapping accuracies of the canopy cover classification of southern yellow pines derived using four data-integration scenarios: Landsat OLI alone; Landsat OLI and Sentinel-1; Landsat OLI with vegetation indices derived from satellite data—normalized difference vegetation index, soil-adjusted vegetation index, modified soil-adjusted vegetation index, transformed soil-adjusted vegetation index, and infrared percentage vegetation index; and 4) Landsat OLI with Sentinel-1 and vegetation indices. The results showed that the integration of Landsat OLI reflectance bands with Sentinel-1 backscattering coefficients and vegetation indices yielded the best overall classification accuracy, about 77%, and standalone Landsat OLI the weakest accuracy, approximately 67%. The findings in this study demonstrate that the addition of backscattering coefficients from Sentinel-1 and vegetation indices positively contributed to the mapping of southern yellow pines.

Introduction

Southern yellow pines such as loblolly pine (*Pinus taeda*), Virginia pine (*P. virginiana*), and shortleaf pine (*P. echinata*) are softwood forest vegetation species commonly found in the southeastern United States. These pine species are commercially marketed and provide economic benefits to the country. For example, loblolly and shortleaf pines are usually grown for pulpwood and sawlogs, whereas Virginia pine is usually grown as Christmas-tree species (English *et al.* 2004; Young *et al.* 2007).

The mapping of softwood forest vegetation species such as loblolly, shortleaf, and Virginia pines is important for effective management of forest resources (Xie *et al.* 2008; Ke *et al.* 2010; Deng *et al.* 2011; Shang and Chisholm 2014; Roth *et al.* 2015). For example, updated digital maps of forest vegetation species and canopy cover are continually being sought by

Clement E. Akumu and Eze O. Amadi are with the Department of Agricultural and Environmental Sciences, College of Agriculture,

Tennessee State University, Nashville, TN 37209-1561
(aclemen1@tnstate.edu).

Contributed by Sidike Paheding, May 3, 2021 (sent for review July 15, 2021; reviewed by Jorge A.S. Centeno, Cary Cox).

forest managers and policy makers to support management decisions and policies (Skidmore *et al.* 1997; Rozenstein and Karniel 2011). Furthermore, forest vegetation canopy cover maps can help to understand tree-species ecology for community dynamics as well as species inputs into the ecosystems (van Ewijk *et al.* 2014). They can also be used as inputs for modeling and other forest management and planning activities such as harvesting, regeneration, and fire management (van Aardt and Wynne 2007; Hamilton *et al.* 2021).

The spectral information of satellite remotely sensed data, such as Landsat Operational Land Imager (OLI) optical data and Sentinel-1 C-band synthetic-aperture radar (SAR) sensor data, make them feasible and cost-effective in mapping forest vegetation canopy cover compared to traditional field-survey methods over large geographic areas (Xie *et al.* 2008; Shang and Chisholm 2014; Vincent *et al.* 2019). However, because many individually sensed images have either high spatial resolution or high spectral resolution, there is a need to integrate satellite remotely sensed data to improve image classification. For example, Jiménez *et al.* (2017) and Fatoyinbo and Armstrong (2010) integrated Landsat Enhanced Thematic Mapper Plus with lidar and National Forest Inventory data to map aboveground forest cover and biomass, and found a more accurate estimation of aboveground forest biomass using this data-integration method. Wan *et al.* (2021) integrated multispectral Sentinel-2 image data with high-spatial-resolution aerial images for tree-species classification of forest stands. They classified and mapped 11 forest vegetation species stands and found an increase in overall mapping accuracy after data integration. Furthermore, Biswas *et al.* (2020) evaluated the contribution of three satellite data sources—Landsat OLI, Sentinel-1, and Sentinel-2—in mapping diverse forest vegetation types in Myanmar. They found that using a combination of Sentinel-1 and Sentinel-2 data produced the highest accuracy (89.6%), followed by Sentinel-2 alone (87.97%) and Landsat OLI (82.68%).

Satellite-derived vegetation indices are useful indicators of forest biophysical condition and can be integrated with satellite remotely sensed data to further improve the discrimination of forest vegetation and canopy cover. This is because spectral vegetation indices measure the photosynthetic size of plant canopies. Furthermore, they are used as indicators to monitor variations in temporal and spatial characteristics of vegetation structure and density (Xue and Su 2017; Akumu *et al.* 2021). For example, Prabhakara *et al.* (2015)

Photogrammetric Engineering & Remote Sensing
Vol. 88, No. 1, January 2022, pp. 29–38
0099-1112/22/29-38

© 2022 American Society for Photogrammetry
and Remote Sensing
doi: 10.14358/PERS.21-00024R2

used vegetation indices to ascertain the correlation between vegetation biomass, ground cover, and derived indices in Maryland (USA). They found a strong correlation between the normalized difference vegetation index (NDVI) and percent vegetation cover. Furthermore, they found the triangular vegetation index most accurate in estimating vegetation biomass. Bera *et al.* (2020) used vegetation indices such as the NDVI, advanced vegetation index, shadow index, and bareness index to detect and monitor forest vegetation canopy cover and health. They found a reduction in forest canopy cover and density between 1998 and 2009 in the Silabati River Basin (India). Furthermore, Reid *et al.* (2016) generated the NDVI from Landsat Thematic Mapper data as an indicator of forest productivity to examine forest cover and health trends at Fort Benning, Georgia. They found that most plots had declining greenness through time, consistent with the overall NDVI trend.

Other recent studies have integrated vegetation indices derived from satellite data with remotely sensed satellite data to map forest canopy cover and habitats (Martinuzzi *et al.* 2008; Sinha *et al.* 2015; Abdollahnejad *et al.* 2019; Ganz *et al.* 2020). For example, Sinha *et al.* (2015) integrated the thermal integrated vegetation index and advanced thermal integrated vegetation index with Landsat Enhanced Thematic Mapper Plus satellite data to map land cover including forest canopy cover in a semi-arid deciduous forest landscape. They found that the classification accuracy of land cover improved with integration of the thermal vegetation indices from the Landsat Enhanced Thematic Mapper Plus thermal band with spectral information. Rhyma *et al.* (2020) integrated Satellite pour l'observation de la Terre (*SPOT*-6 and *SPOT*-7) satellite data with the NDVI and soil-adjusted vegetation index (SAVI) to discriminate forest canopy cover. They found satellite data-derived vegetation indices useful in improving the accuracy of classification in a mangrove forest ecosystem. Although satellite-derived vegetation indices and satellite data have been integrated in forest canopy cover classification, there is no known knowledge of the integration of Landsat OLI optical data with *Sentinel-1* C-band SAR sensor data and derived vegetation indices for mapping forest canopy cover of southern yellow pines. The integration of Landsat OLI optical data with *Sentinel-1* microwave satellite data and derived vegetation indices could improve the overall detection, mapping, and classification accuracy of the canopy cover of southern yellow pines.

The overall aim of this study is to examine the integration of Landsat OLI optical data with *Sentinel-1* C-band SAR sensor satellite data and derived vegetation indices in mapping the canopy cover of southern yellow pines (loblolly, shortleaf, and Virginia pines). Specifically, this study assesses the overall mapping accuracies of the canopy cover classification of southern yellow pines derived using four data-integration scenarios: Landsat OLI alone; Landsat OLI and *Sentinel-1*; Landsat OLI with satellite data-derived vegetation indices—NDVI, SAVI, modified soil-adjusted vegetation index (MSAVI), transformed soil-adjusted vegetation index (TSavi), infrared percentage vegetation index (IPVI); and Landsat OLI with *Sentinel-1* and satellite data-derived vegetation indices. To the best of our knowledge, this is the first study to examine the integration of satellite data-derived vegetation indices with Landsat OLI optical and *Sentinel-1* C-band SAR sensor data in the classification and mapping of the canopy cover of southern yellow pines.

Materials and Methods

Study Area

Marion County, Tennessee, was selected as a case study area in this study (Figure 1). It is located between latitude 35.319°N and 34.984°N and longitude 85.361°W and 85.872°W. The county is in the southern

region of Tennessee and occupies approximately 516 mi² of surface area. This study area was selected because of the availability of cloud-free Landsat OLI satellite data and several field data sets of southern yellow pines.

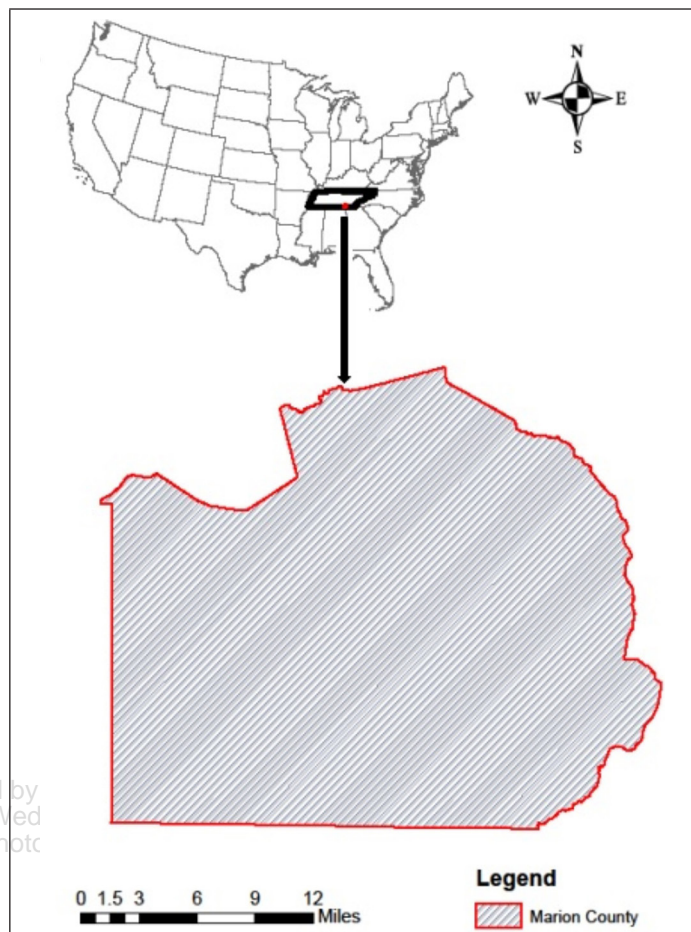


Figure 1. Study area: Marion County, Tennessee, United States of America.

Vegetation

A significant part of the study area is covered by forest vegetation, especially softwood forest vegetation such as southern yellow pines. Southern yellow pines commonly found in the region included loblolly pine (*P. taeda*), Virginia pine (*P. virginiana*), and shortleaf pine (*P. echinata*). In addition to softwood forest vegetation, there is also hardwood forest vegetation in the area, with common species including locust (*Gleditsia* spp.), poplar (*Populus* spp.), maple (*Acer* spp.), oak (*Quercus* spp.), elm (*Ulmus* spp.), hickory (*Carya* spp.), and sycamore (*Platanus* spp.); Akumu *et al.* 2018).

Climate

The climate of the region is characterized by hot summers and moderately cold winters with some erratic cold spells and snowfall (Akumu *et al.* 2018; Hodges *et al.* 2018). The seasonal average temperatures are 41°F in the winter, 60°F in the spring, 78°F in the summer, and 60°F in the fall (Hinkle 1989). The mean annual temperature of Marion County is about 78°F. Average precipitation in the region is about 51 in. (1300 mm), evenly distributed over the seasons (Hodges *et al.* 2018).

Geology

Marion County is on the Cumberland Plateau and contains a good portion of Sequatchie Valley and part of the Tennessee River. The plateau is formed by level rocks. The tableland

of the Cumberland Plateau, Walden Ridge, and the Raccoon Mountain crest are capped by sandstones, shales, conglomerates, and coal seams (Hodges *et al.* 2018). The Tennessee and Sequatchie River floors are made of limestones of Ordovician and Mississippian origin which contain alkaline soils (Akumu *et al.* 2018). The most noticeable landform in the county is Sequatchie Valley, which runs northeast to southwest through the center of the county. The valley is linear and covers about 25% of the total area of the county (Starnes 1986).

Methodology

The methodology for this study involved six data-processing: acquisition of Landsat OLI optical data and *Sentinel-1* microwave satellite data; preprocessing of satellite data; generation of satellite-data vegetation indices; data integration; classification of the canopy cover of southern yellow pines; and validation/accuracy assessment (Figure 2).

The Landsat OLI satellite data, with an acquisition date of 28 February 2016, were downloaded from the United States Geological Survey website (<http://earthexplorer.usgs.gov>) as a Level-1 cloud-free scene. Landsat OLI satellite data have 11 spectral bands, with a spatial resolution of 30 m for bands 1–7 and 9 (Table 1). Bands 1–7 were used in the classification and mapping of the canopy cover of southern yellow pines.

This study selected a Landsat OLI satellite data set with a winter acquisition date because southern yellow pines are conifers that are easily detected in the winter season, when deciduous trees shed their leaves. The Landsat OLI scene with 30-m spatial resolution was subsetted for the study area and geometric correction was performed. The geometric correction was carried out using more than 50 ground control points with a root-mean-square (RMS) error < 1 pixel. The RMS error is the distance between the input (source) location of

a ground control point and the transformed location of the same ground control point (Tawfeik *et al.* 2016). Using more than 50 ground control points is acceptable if the RMS error is < 1 pixel, but unacceptable if it is > 1 pixel (Nguyen 2015; Pehani *et al.* 2016; Tawfeik *et al.* 2016). This is because an RMS error < 1 pixel provides a high-quality georeferenced image compared to an RMS error > 1 pixel (Baboo *et al.* 2011; Tawfeik *et al.* 2016).

Radiometric correction was performed on the Landsat OLI satellite data by converting digital numbers to at-surface reflectance. It entails correcting image pixel values for variation in the sun elevation angle and calibrating images to account for degradation of the sensor over time. Changes in sensor calibration factors will obscure real changes on the ground

Table 1. Landsat Operational Land Imager spectral bands and characteristics.

Band	Wavelength (μm)	Resolution (m)
1: Ultra Blue (coastal/aerosol)	0.43–0.45	30
2: Blue	0.45–0.51	30
3: Green	0.53–0.59	30
4: Red	0.64–0.67	30
5: Near-infrared	0.85–0.88	30
6: Shortwave infrared 1	1.57–1.65	30
7: Shortwave infrared 2	2.11–2.29	30
8: Panchromatic	0.50–0.68	15
9: Cirrus	1.36–1.38	30
10: Thermal infrared 1	10.60–11.19	100 × 30
11: Thermal infrared 2	11.50–12.51	100 × 30

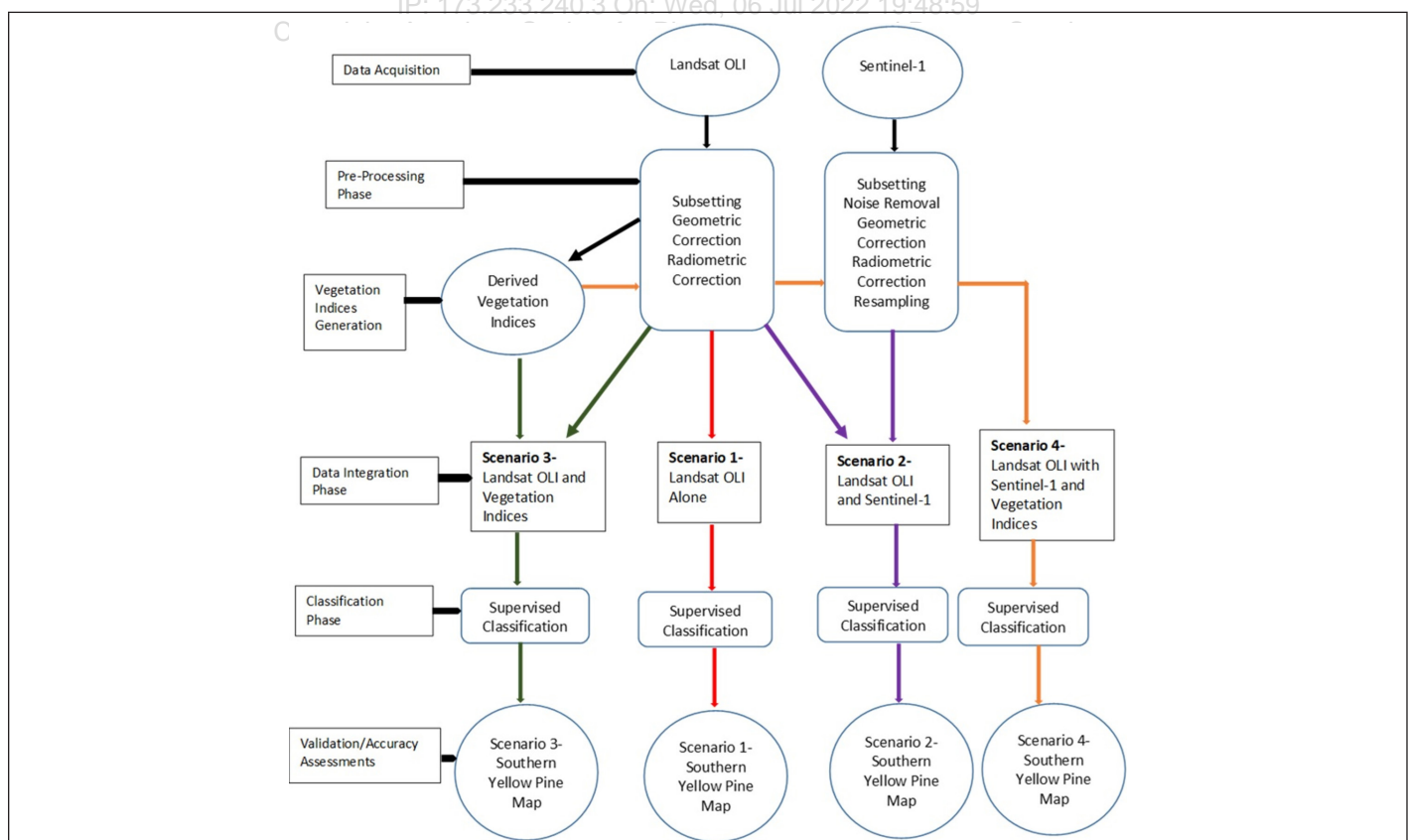


Figure 2. A schematic representation of the methodology used to classify southern yellow pines using four data-integration methods.

(Mather and Koch 2011). The Landsat OLI scene was converted from digital numbers to at-surface reflectance by using reflectance rescaling coefficients derived by the United States Geological Survey (2019):

$$\rho\lambda' = M_p Q_{\text{cal}} + A_p \quad (1)$$

where $\rho\lambda'$ = top-of-atmosphere (TOA) planetary reflectance without correction for solar angle, M_p = band-specific multiplicative rescaling factor (Reflectance_Mult_Band_x, where x is the band number), A_p = band-specific additive rescaling factor (Reflectance_Add_Band_x), and Q_{cal} = digital numbers. The factors Reflectance_Mult_Band_x and Reflectance_Add_Band_x were obtained from the header file of the imagery.

Furthermore, the correction of TOA planetary reflectance for sun angle was performed using the equation (United States Geological Survey 2019)

$$\rho\lambda = \rho\lambda'/\sin(\theta_{\text{SE}}) \quad (2)$$

where $\rho\lambda$ = TOA planetary reflectance corrected for sun angle, $\rho\lambda'$ = TOA planetary reflectance without correction for solar angle, and θ_{SE} = local sun elevation angle (in degrees), provided in the metadata (Sun_Elevation).

The *Sentinel-1* C-band SAR sensor satellite data, with an acquisition date of 24 January 2018, were downloaded from the European Space Agency Data Hub (<https://scihub.copernicus.eu/dhus/#/home>) as a *Sentinel-1A* scene. *Sentinel-1* has a C-band with four acquisition modes: Stripmap, Interferometric Wide swath, Extra Wide swath, and Wave (Table 2). The Interferometric Wide swath mode vertical-vertical, vertical-horizontal, horizontal-vertical, and horizontal-horizontal polarizations was used in the classification and mapping of the canopy cover of southern yellow pines.

Table 2. Mode, spectral resolution, swath, and polarization of *Sentinel-1* C-band SAR sensor.

Mode	Swath			
	Incidence Angle (°)	Resolution (m)	Width (km)	Polarization
Stripmap	20–45	5×5	80	HH+HV, VH+VV, HH, VV
Interferometric Wide swath	29–46	5×20	250	HH+HV, VH+VV, HH, VV
Extra Wide swath	19–47	20×40	400	HH+HV, VH+VV, HH, VV
Wave	22–35 35–38	5×5	20×20	HH, VV

H = horizontal; V = vertical.

The *Sentinel-1* microwave scene with a spatial resolution of 5×20 m was subsetted to the study area and noise removal (speckle filtering) was performed. The noise removal was carried out using spatial averaging in a 60×60-m window. Geometric correction was performed on the scene using the Shuttle Radar Topography Mission global digital elevation map for the study area. The digital elevation map was used to provide terrain correction, and the *Sentinel-1* data were reprojected to the WGS84 - UTM Zone 16 map projection. Radiometric correction was performed on the imagery by converting the digital numbers to backscattering coefficients (σ^o ; Twele *et al.* 2016):

$$\sigma^o = \frac{\text{DN}^2 \sin \theta}{K} \quad (3)$$

where θ = incidence angle, K = calibration constant, and DN = digital numbers.

The backscattering coefficients were then expressed in decibels (Twele *et al.* 2016):

$$\sigma^o_{\text{dB}} = 10 \log_{10}(\sigma^o) \quad (4)$$

The scene was later resampled to the same spatial resolution as the Landsat OLI satellite data—30-m cell size.

The TOA reflectance image of the Landsat OLI satellite data was used to generate the NDVI, SAVI, MSAVI, TSAVI, and IPVI. These indices were selected because they are indicators of plant greenness and are considered to take into account the effect of soil background. For example, these indices have a spectral red band that is strongly absorbed by plant chlorophyll and is an indicator of vegetation greenness. Furthermore, they also have an infrared band that is strongly absorbed when plants become stressed by factors such as dehydration, lack of nutrients, diseases, and leaf-structure deterioration (Qi *et al.* 1994; Lichtenhaller *et al.* 1996). In addition, the TSAVI has an adjustment factor to minimize the effect of soil background (Baret *et al.* 1989). The vegetation indices were also selected because they can be easily generated from the Landsat OLI spectral bands and could contribute to the discrimination of southern yellow pines. Other indices, such as the normalized difference water index and modified normalized difference water index, were not considered because they have shortwave infrared bands and are good indicators of vegetation wetness rather than greenness (Gao 1996; Xu 2006).

The normalized difference vegetation index was generated as (Lichtenhaller *et al.* 1996)

$$\text{NDVI} = \frac{\text{Near-infrared} - \text{Red}}{\text{Near-infrared} + \text{Red}} \quad (5)$$

The soil-adjusted vegetation index was generated using (Huete 1988)

$$\text{SAVI} = \frac{(\text{Near-infrared} - \text{Red})(1+L)}{(\text{Near-infrared} + \text{Red} + L)} \quad (6)$$

where L is the soil brightness conversion factor of 0.5.

The modified soil-adjusted vegetation index was generated using (Qi *et al.* 1994)

$$\text{MSAVI} = \frac{(\text{Near-infrared} - \text{Red})(1+L)}{\text{Near-infrared} + \text{Red} + L} \quad (7)$$

where L is calculated by

$$L = 1 - \frac{2 * s * (\text{Near-infrared} - \text{Red}) * (\text{Near-infrared} - s * \text{Red})}{(\text{Near-infrared} + \text{Red})} \quad (8)$$

in which s is the slope of the soil line from a plot of brightness values of red versus near-infrared.

The transformed soil-adjusted vegetation index was generated using (Baret *et al.* 1989)

$$\text{TSAVI} = \frac{a(\text{NIR} - a * \text{Red} - b)}{[\text{Red} + a(\text{NIR} - b) + 0.08(1+a^2)]} \quad (9)$$

where a and b are the slope and intercept of the soil line, respectively; 0.08 is the adjusted coefficient value; and NIR is the near-infrared value.

The infrared percentage vegetation index was generated using (Crippen 1990):

$$IPVI = \frac{\text{Near-infrared}}{\text{Near-infrared} + \text{Red}} \quad (10)$$

First, the stand-alone Landsat OLI reflectance scene was used to classify and map the canopy cover of southern yellow pines, as scenario 1. The Landsat OLI visible and infrared spectral bands were used in classifying the canopy cover of southern yellow pines. Second, the Landsat OLI reflectance scene was integrated with *Sentinel-1* backscattering coefficients to classify and map southern yellow pines, as scenario 2. Third, the Landsat OLI reflectance scene was integrated with the derived vegetation indices NDVI, SAVI, MSAVI, TSAVI, and IPVI to classify and map southern yellow pines, as scenario 3. Fourth, the Landsat OLI reflectance scene was integrated with *Sentinel-1* backscattering coefficients and derived vegetation indices to classify and map southern yellow pines, as scenario 4. The spectral bands of the Landsat OLI reflectance scene were integrated directly as separate bands with *Sentinel-1* backscattering coefficients and derived vegetation indices.

Supervised classification was performed to classify and map the canopy cover of southern yellow pines in all four data-integration scenarios. The canopy cover of loblolly, shortleaf, and Virginia pines was classified and mapped using training data from 22 field sites. The southern yellow pines on each field site covered a large geographic area of >200,000 m². The sites represented homogenous stands of loblolly, shortleaf, and Virginia pines. Most of the southern yellow pines at the field sites were at least 6 m tall. There were seven sites of loblolly pine, 12 of shortleaf, and three of Virginia pine. The site-location data were obtained from area foresters at the Tennessee Department of Agriculture. Sixty polygons (20 loblolly, 20 shortleaf, and 20 Virginia pine) were digitized from the 22 field sites to serve as training data in the supervised classification process.

The supervised classification was performed using a machine-learning random-forest classification algorithm, with the 60 digitized polygons of southern yellow pines serving as training data. The random-forest classification model was controlled for overfitting by five-fold cross-validation repeated twice on the training data. During the cross-validation process, about 25% of the training data were kept aside as test data set. The remaining 75%—the training data set—was divided into five equal sets and used in the five-fold cross-validation. The first set was kept as the holdout (testing) set and the remaining sets were used to train the random-forest classification prediction model of southern yellow pines. The five-fold cross-validation was performed with a changing holdout (testing) set. The mean accuracy of the canopy cover classification of southern yellow pines generated from the five-fold cross-validation process was estimated. The training data were then used in the random-forest classification of the canopy cover of southern yellow pines, and the kept-aside 25% test data set was used to validate the classification. The accuracy with the test and training data sets was then evaluated (Sharma *et al.* 2017; Costa *et al.* 2018; Elmaz *et al.* 2020).

Furthermore, the numbers of trees and training samples in the random-forest classification prediction model were selected through a resampling-based procedure to search for optimal tuning parameters. The optimal settings were selected based on the mean overall accuracy across the five-fold cross-validation, repeated twice (Sharma *et al.* 2017; Costa *et al.* 2018). The default number of training samples was selected and set at 5000, and the number of random-forest trees was set at 10. The random-forest classification algorithm was selected because it

has been found to outperform other machine-learning classification algorithms such as support vector machines in mapping forest canopy cover and species (Shang and Chisholm 2014; Sharma *et al.* 2017; Elmahdy *et al.* 2020; Sjöqvist *et al.* 2020).

The canopy cover maps of southern yellow pines generated using the four data-integration classification methods were validated to examine how well they represented southern yellow pines on the ground. The validation effort was performed by randomly selecting 100 polygons from each classified canopy cover map. The validation data (100 polygons) were distinct from the training data (60 polygons) used in the random-forest classification of the canopy cover of southern yellow pines.

Determination of ground truth by field-plot visits and use of Google Earth Pro information was used to validate the classified canopy cover maps derived from the four data-integration scenarios. The overall accuracy was computed for each classified map by dividing the total correct (the sum of the major diagonal in the error matrix table) by the total number of pixels in the error matrix table (Mather and Koch 2011). The κ coefficient was also measured as described by Mather and Koch (2011). The classified canopy cover maps were later exported into Geographic Information System for extent analyses.

Results and Discussion

The canopy cover of southern yellow pines representing loblolly, shortleaf, and Virginia pines (Figures 3–6) was successfully classified and mapped using the four data-integration classification methods. The distribution of loblolly, shortleaf, and Virginia pines was similar in all four scenarios. The canopy cover of shortleaf pine was more intense in the northern parts of the study area than the southern parts. Similarly, the canopy cover of loblolly and Virginia pines was more abundant in the northern parts of the study area than the southern portions. The lesser canopy cover of southern yellow pines in the southern parts of the study area is likely because of intense harvesting. Southern yellow pines are continually harvested as pulpwood and saw timber products in the region (Clabo and Clatterbuck 2005; Hansen *et al.* 2014). Furthermore, on average, shortleaf pine had the most canopy cover with all four data-integration classification methods, and Virginia pine had the least canopy cover (Table 3). The dry, better-drained ridgetops associated with the Cumberland Plateau, which are commonly found in the region, possibly provided suitable conditions for growing shortleaf pines (Hodges *et al.* 2018).

The overall, user, and producer accuracies varied in all data-integration scenarios. The overall accuracy is the average of the individual class accuracies expressed as a percentage (Mather and Koch 2011). The user accuracy is a measure of how well the classified canopy cover of loblolly, shortleaf, and Virginia pines on the map represented southern yellow pines on the ground. The producer accuracy is the ability of the random-forest classification algorithm to detect southern yellow pines.

Table 3. Percentage canopy cover of loblolly, shortleaf, and Virginia pines derived with the four data-integration classification methods.

Southern Yellow Pine	Scenario 1: Landsat OLI Alone	Scenario 2: Landsat OLI and Sentinel-1 Data	Scenario 3: Landsat OLI and Vegetation Indices	Scenario 4: Landsat OLI with <i>Sentinel-1</i> Data and Vegetation Indices
Loblolly	14	17	23	14
Shortleaf	71	73	62	73
Virginia	15	10	15	13

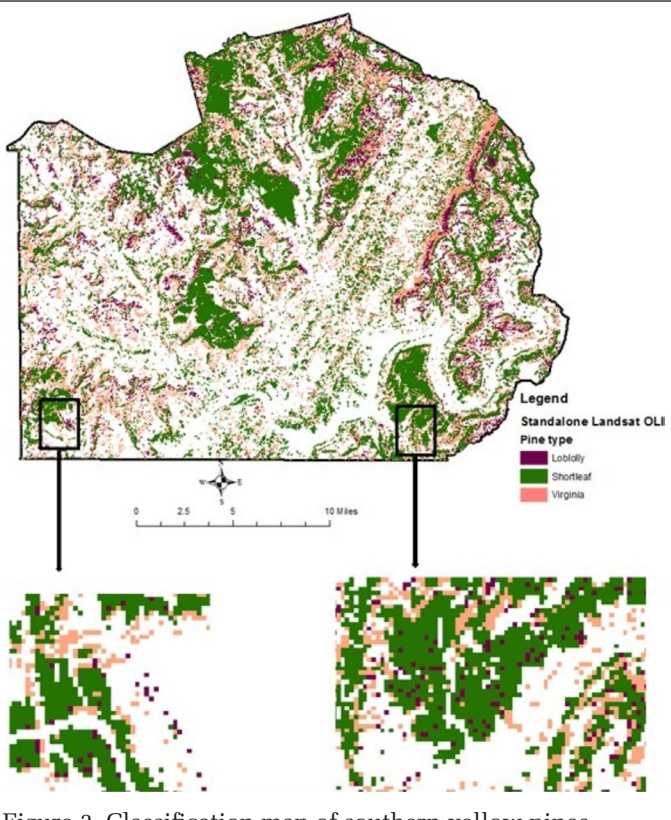


Figure 3. Classification map of southern yellow pines (loblolly, shortleaf, and Virginia pines) derived from stand-alone Landsat OLI satellite data (scenario 1).

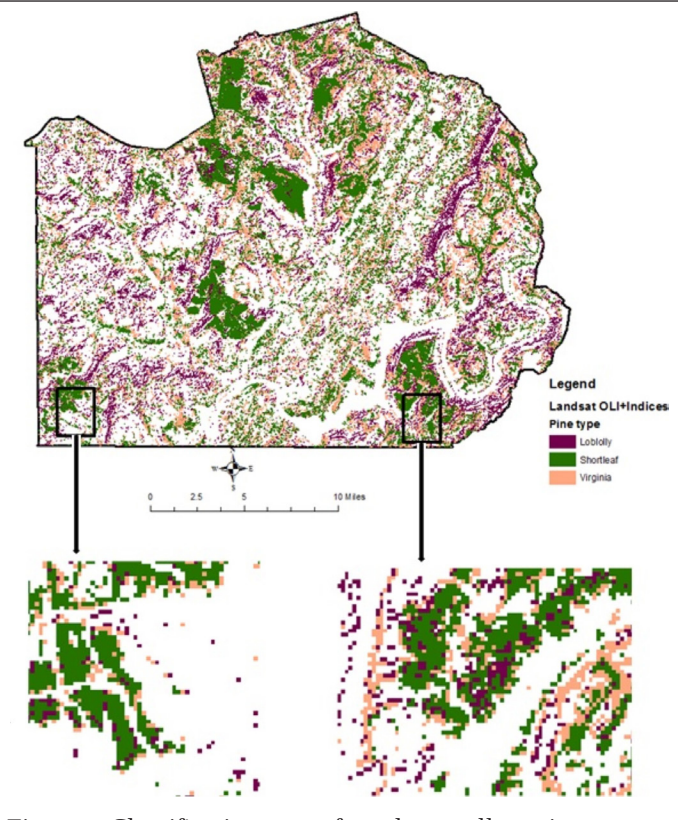


Figure 5. Classification map of southern yellow pines (loblolly, shortleaf, and Virginia pines) derived from the integration of Landsat OLI data and derived vegetation indices (scenario 3).

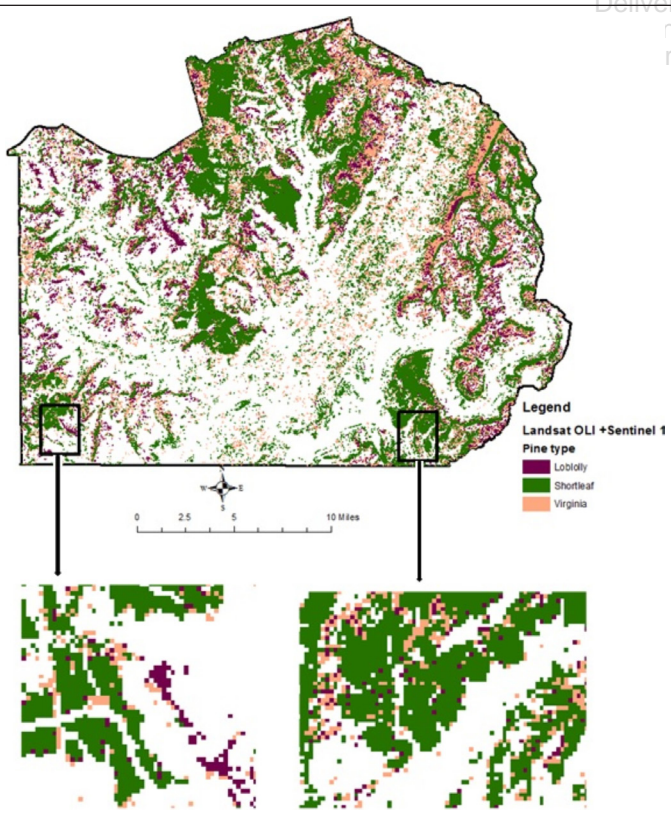


Figure 4. Classification map of southern yellow pines (loblolly, shortleaf, and Virginia pines) derived from the integration of Landsat OLI optical and *Sentinel-1* microwave satellite data (scenario 2).

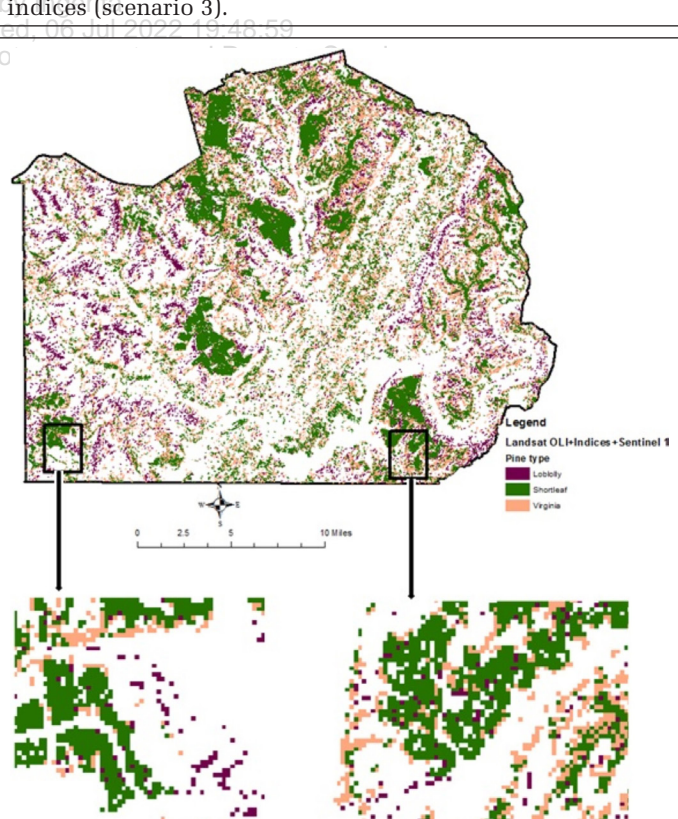


Figure 6. Classification map of southern yellow pines (loblolly, shortleaf, and Virginia pines) derived from the integration of Landsat OLI and *Sentinel-1* data with derived vegetation indices (scenario 4).

Table 4. Classification accuracies of the canopy cover of southern yellow pines derived using four data-integration classification methods.

User Accuracy (%)				
Southern Yellow Pine Class	Landsat OLI Alone (Scenario 1)	Landsat OLI with Sentinel-1 Data (Scenario 2)	Landsat OLI with Derived Vegetation Indices (Scenario 3)	Landsat OLI with <i>Sentinel-1</i> Data and Derived Vegetation Indices (Scenario 4)
Loblolly	67	70	87	83
Shortleaf	70	73	75	80
Virginia	63	67	63	67
Producer Accuracy (%)				
Southern Yellow Pine Class	Landsat OLI Alone (Scenario 1)	Landsat OLI with Sentinel-1 Data (Scenario 2)	Landsat OLI with Derived Vegetation Indices (Scenario 3)	Landsat OLI with <i>Sentinel-1</i> Data and Derived Vegetation Indices (Scenario 4)
Loblolly	65	66	72	76
Shortleaf	62	66	71	73
Virginia	79	83	86	87
Overall Accuracy (%)				
Landsat OLI Alone (Scenario 1)	Landsat OLI with Sentinel-1 Data (Scenario 2)	Landsat OLI with Derived Vegetation Indices (Scenario 3)	Landsat OLI with <i>Sentinel-1</i> Data and Derived Vegetation Indices (Scenario 4)	
67	70	75	77	
κ Statistics				
Landsat OLI Alone (Scenario 1)	Landsat OLI with Sentinel-1 Data (Scenario 2)	Landsat OLI with Derived Vegetation Indices (Scenario 3)	Landsat OLI with <i>Sentinel-1</i> Data and Derived Vegetation Indices (Scenario 4)	
0.5	0.54	0.62	0.65	

The overall classification accuracy of the canopy cover of southern yellow pines was about 67% when the stand-alone Landsat OLI satellite data set was used (scenario 1; Tables 4 and 5). In this classification method, the user accuracy was highest (70%) for shortleaf pine and lowest (63%) for Virginia pine. In contrast, the producer accuracy was highest (79%) for Virginia pine and lowest (62%) for shortleaf pine (Table 4).

In the classification method in which the Landsat OLI reflectance scene was integrated with *Sentinel-1* backscattering coefficients (scenario 2), the overall accuracy was about 70% compared to reference data (Tables 4 and 6). The overall accuracy increased by about 5% relative to the stand-alone Landsat OLI satellite data. Similarly, other studies have found weaker performance using stand-alone Landsat OLI data in forest canopy cover prediction and mapping compared to integrating Landsat OLI data with *Sentinel-1* microwave data (Poortinga *et al.* 2019; Biswas *et al.* 2020; Li *et al.* 2020). In scenario 2, the user accuracy was highest (73%) for shortleaf and lowest (67%) for Virginia pine. Both loblolly and shortleaf pines had similar producer accuracies, of about 66%, whereas Virginia pine had a producer accuracy of approximately 83% (Table 4). Furthermore, when *Sentinel-1* backscattering coefficients were integrated with Landsat OLI reflectance bands, Virginia pine had a 4% gain in user accuracy, and shortleaf and loblolly pines had a 3% gain. The similar gains in user accuracy imply that the addition of *Sentinel-1* backscattering coefficients is useful for better characterizing loblolly, shortleaf, and Virginia pines. In contrast, shortleaf and Virginia pines had a 4% gain in producer accuracy when *Sentinel-1* backscattering coefficients were integrated, whereas loblolly pine had a 1% gain.

In the classification method in which the Landsat OLI reflectance scene was integrated with satellite-derived vegetation indices (scenario 3), the overall classification accuracy was around 75% compared to reference data (Tables 4 and 7). The overall mapping accuracy of the canopy cover of southern yellow pines increased by about 12% relative to stand-alone Landsat OLI satellite data. Similarly, the results of Matongera *et al.* (2017) also showed that integrating Landsat OLI data with vegetation indices yielded better overall classification accuracy than stand-alone Landsat OLI satellite data. In scenario 3, the user accuracy was highest (87%) for loblolly

Table 5. Error matrix table for the classification of southern yellow pines using stand-alone Landsat OLI satellite data (scenario 1).

Class	Loblolly	Shortleaf	Virginia	Total
Reference				
Loblolly	20	8	2	30
Shortleaf	9	28	3	40
Virginia	2	9	19	30
Total	31	45	24	100

Table 6. Error matrix table for the classification of southern yellow pines using integrated Landsat OLI and *Sentinel-1* satellite data (scenario 2).

Class	Loblolly	Shortleaf	Virginia	Total
Reference				
Loblolly	21	7	2	30
Shortleaf	9	29	2	40
Virginia	2	8	20	30
Total	32	44	24	100

Table 7. Error matrix table for the classification of southern yellow pines using integrated Landsat OLI data and satellite-derived vegetation indices (scenario 3).

Class	Loblolly	Shortleaf	Virginia	Total
Reference				
Loblolly	26	3	1	30
Shortleaf	8	30	2	40
Virginia	2	9	19	30
Total	36	42	22	100

Table 8. Error matrix table for the classification of southern yellow pines using integrated Landsat OLI and *Sentinel-1* satellite data and derived vegetation indices (scenario 4).

Class	Loblolly	Shortleaf	Virginia	Total
Reference				
Loblolly	25	4	1	30
Shortleaf	6	32	2	40
Virginia	2	8	20	30
Total	33	44	23	100

and lowest (63%) for Virginia pine. The producer accuracy was highest (86%) for Virginia pine and lowest (71%) for shortleaf pine (Table 4). Furthermore, loblolly pine had the greatest gain in user accuracy (20%), and Virginia pine the least (0%). This implies that the addition of vegetation indices is useful for better characterizing loblolly pine relative to shortleaf and Virginia pines. In contrast, shortleaf pine had the greatest gain in producer accuracy (9%), and loblolly and Virginia pines the least (7%).

In the classification method in which the Landsat OLI reflectance scene was integrated with *Sentinel-1* backscattering coefficients and derived vegetation indices (scenario 4), the overall classification accuracy of southern yellow pines was approximately 77% compared to reference data (Tables 4 and 8). The overall mapping accuracy of the canopy cover of southern yellow pines increased by about 15% compared to stand-alone Landsat OLI satellite data. In scenario 4, the user accuracy was highest (83%) for loblolly and lowest (67%) for Virginia pine. The producer accuracy was highest (87%) for Virginia pine and lowest (73%) for shortleaf pine (Table 4). Furthermore, loblolly pine had the highest gain in user accuracy (16%) in scenario 4 compared to scenario 1, whereas Virginia pine had the lowest (4%). Likewise, both shortleaf and loblolly pines had the highest gain in producer accuracy (11%), and Virginia pine the lowest (8%).

The lower gain in user accuracy for Virginia pine relative to shortleaf and loblolly pines with the addition of *Sentinel-1* backscattering coefficients and derived vegetation indices is possibly due to the morphology of Virginia pine. It has a similar bark color to shortleaf pine—a mix of reddish brown (United States Department of Agriculture 2021)—which possibly increased confusion between Virginia and shortleaf pines in the classification. Consequently, about 27% of Virginia pine was incorrectly classified on the map in scenario 4. Nonetheless, scenario 4 yielded the best overall classification accuracy of the canopy cover of southern yellow pines, whereas the use of stand-alone Landsat OLI data (scenario 1) produced the weakest overall accuracy results in the classification and mapping of the canopy cover of southern yellow pines. Scenario 4 achieved the best overall accuracy because the addition of *Sentinel-1* backscattering coefficients and vegetation indices to Landsat OLI reflectance data improved the spectral resolution and variability of the input variables in the classification. This likely improved the predictive capability of the random-forest classification algorithm. Hence, the addition of backscattering coefficients from *Sentinel-1* and satellite-derived vegetation indices positively contributed to the classification and mapping of the canopy cover of loblolly, shortleaf, and Virginia pines.

Based on the feature-importance score—which estimates which variables were important in the classification process—Landsat OLI spectral band 6 and MSAVI had the highest scores, ranked first and second, respectively. In contrast, IPVI and TSAVI had the lowest scores, ranked fifteenth and sixteenth, respectively. This means that Landsat OLI spectral band 6 and MSAVI were the most important input variables and had high contributions to the classification, whereas IPVI and TSAVI were the least relevant input variables and had low contributions. Therefore, not all the satellite data-derived vegetation indices are necessary in classifying and mapping southern yellow pines using the random-forest classification algorithm. Using just three of the vegetation indices—MSAVI, NDVI, and SAVI—will be enough to improve the classification and mapping of the canopy cover of southern yellow pines. Landsat OLI spectral bands 1 through 5 and 7, the *Sentinel-1* microwave C-band VV, VH, HV, and HH polarizations, NDVI, and SAVI had medium relevance and contributions to the classification, ranked between second and fifteenth based on

their feature-importance scores. Therefore, out of the 16 input variables used in the classification process, 14 were relevant and necessary to improve the classification and mapping of southern pines. The use of the random-forest algorithm was better in the data-integration classification methods than the use of other machine-learning algorithms, such as support vector machine, because it provided estimates of the importance of each input variable in the classification process and could be used as a feature-selection tool.

In this study, the 7% decrease in overall classification accuracy of southern yellow pines produced by integrating Landsat OLI data with *Sentinel-1* backscattering coefficients compared to using vegetation indices was not expected. This implies that vegetation indices could contribute more to the classification and mapping of the canopy cover of southern yellow pines than *Sentinel-1* backscattering coefficients. However, to attain the best prediction and mapping of the canopy cover of loblolly, shortleaf, and Virginia pines, the integration of the Landsat OLI reflectance scene with *Sentinel-1* backscattering coefficients and derived vegetation indices is relevant.

Future research will examine how other machine-learning classification algorithms, such as gradient-boosted tree, extreme gradient boosting, and multi-layer perceptron, perform against the random-forest classifier in mapping southern yellow pines using the Landsat OLI reflectance scene with *Sentinel-1* backscattering coefficients and derived vegetation indices. Furthermore, exploring the integration of Landsat OLI optical data with *Sentinel-1* C-band SAR sensor and lidar data in other natural-resources applications, such as wetlands and agriculture, is an area of further research.

Conclusion

This study successfully examined the integration of Landsat OLI optical data with *Sentinel-1* microwave satellite data and derived vegetation indices in mapping the canopy cover of loblolly, shortleaf, and Virginia pines. We found that when Landsat OLI data was integrated with *Sentinel-1* backscattering coefficients, the classification of the canopy cover of southern yellow pines increased by about 5% compared to stand-alone Landsat OLI satellite data. Similarly, the integration of Landsat OLI reflectance bands with satellite data-derived vegetation indices increased the overall mapping accuracy by about 12% compared to stand-alone Landsat OLI satellite data. Furthermore, the best overall classification accuracy (77%) of the canopy cover of southern yellow pines was produced when the Landsat OLI reflectance scene was integrated with *Sentinel-1* backscattering coefficients and derived vegetation indices. Landsat OLI spectral band 6 and MSAVI were the most important input variables in the classification of the canopy cover, and IPVI and TSAVI were the least important variables. The classification method that integrated Landsat OLI optical data with *Sentinel-1* microwave satellite data and derived vegetation indices can be easily developed to successfully map the canopy cover of southern yellow pines.

Acknowledgments

Many thanks to Jim D. Lane at Prentice Cooper State Forest and Brian Huggett at the Tennessee Department of Agriculture, Forestry Section, for providing the field-location data set used to carry out this project. Our appreciation goes to the United States Department of Agriculture for providing support through the McIntire-Stennis funding program.

References

- Abdollahnejad, A., D. Panagiotidis and L. Bilek. 2019. An integrated GIS and remote sensing approach for monitoring harvested areas from very high-resolution, low-cost satellite images. *Remote Sensing* 11(21):2539.
- Akumu, C. E., E. O. Amadi and S. Dennis. 2021. Application of drone and WorldView-4 satellite data in mapping and monitoring grazing land cover and pasture quality: Pre- and post-flooding. *Land* 10(3):321.
- Akumu, C. E., J. Henry, T. S. Gala, S. Dennis, C. Reddy, F. Tegegne, S. Haile and R. S. Archer. 2018. Inland wetlands mapping and vulnerability assessment using an integrated geographic information system and remote sensing techniques. *Global Journal of Environmental Science and Management* 4(4):387–400.
- Baret, F., G. Guyot and D. J. Major. 1989. TSAVI: A vegetation index which minimizes soil brightness effects on LAI and APAR estimation. Pages 1355–1358 in *12th Canadian Symposium on Remote Sensing Geoscience and Remote Sensing Symposium*, held in Vancouver, British Columbia, 10–14 July 1989. Edited by J. Editor. Location: IEEE.
- Bera, B., S. Saha and S. Bhattacharjee. 2020. Estimation of forest canopy cover and forest fragmentation mapping using Landsat satellite data of Silabati River Basin (India). *KN—Journal of Cartography and Geographic Information* 70:181–197.
- Biswas, S., Q. Huang, A. Anand, M. S. Mon, F.-E. Arnold and P. Leimgruber. 2020. A multi sensor approach to forest type mapping for advancing monitoring of Sustainable Development Goals (SDG) in Myanmar. *Remote Sensing* 12(19):3220.
- Clabo, D. C. and W. Clatterbuck, eds. 2005. *A Tennessee Landowner and Practitioner Guide for Establishment and Management of Shortleaf and Other Pines*. Publication PB1751. Location: University of Tennessee Extension, Institute of Agriculture.
- Costa, H., D. Almeida, F. Vala, F. Marcelino and M. Caetano. 2018. Land cover mapping from remotely sensed and auxiliary data for harmonized official statistics. *ISPRS International Journal of Geo-Information* 7(4):157. <https://doi.org/10.3390/jigi7040157>.
- Crippen, R. E. 1990. Calculating the vegetation index faster. *Remote Sensing of Environment* 34(1):71–73.
- Deng, S., Y. Shi, Y. Jin and L. Wang. 2011. A GIS-based approach for quantifying and mapping carbon sink and stock values of forest ecosystem: A case study. *Energy Procedia* 5:1535–1545.
- Elmahdy, S. I., T. A. Ali, M. M. Mohamed, F. M. Howari, M. Abouleish and D. Simonet. 2020. Spatiotemporal mapping and monitoring of mangrove forests changes from 1990 to 2019 in the Northern Emirates, UAE using random forest, kernel logistic regression and naive Bayes tree models. *Frontiers in Environmental Science* 8:102. <https://doi.org/10.3389/fenvs.2020.00102>.
- Elmaz, F., B. Büyüçakır, Ö. Yücel and A. Y. Mutlu. 2020. Classification of solid fuels with machine learning. *Fuel* 266:117066. <https://doi.org/10.1016/j.fuel.2020.117066>.
- English, B., J. Menard and K. Jensen. 2004. *Tennessee's Forest and Forest Products Industry and Associated Economic Impacts for 2000*. Research Series 01-04. Knoxville, Tenn.: The University of Tennessee, Agricultural Experiment Station.
- Fatoyinbo, T. E. and A. H. Armstrong. 2010. Remote characterization of biomass measurements: Case study of mangrove forests. In *Biomass*, edited by M. Momba and F. Bux, 65–78. Rjeka, Croatia: InTech.
- Ganz, S., P. Adler and G. Kändler. 2020. Forest cover mapping based on a combination of aerial images and Sentinel-2 satellite data compared to National Forest Inventory data. *Forests* 11:1322.
- Gao, B.-C. 1996. NDWI—A normalized difference water index for remote sensing of vegetation liquid water from space. *Remote Sensing of Environment* 58(3):257–266.
- Hamilton, D. A., K. L. Brothers, S. D. Jones, J. Colwell and J. Winters. 2021. Wildland fire tree mortality mapping from hyperspatial imagery using machine learning. *Remote Sensing* 13(2):290.
- Hansen, M. C., A. Egorov, P. V. Potapov, S. V. Stehman, A. Tyukavina, S. A. Turubanova, D. P. Roy, S. J. Goetz, T. R. Loveland, J. Ju, A. Kommareddy, V. Kovalskyy, C. Forsyth and T. Bents. 2014. Monitoring conterminous United States (CONUS) land cover change with Web-Enabled Landsat Data (WELD). *Remote Sensing of the Environment* 140:466–484.
- Hinkle, C. R. 1989. Forest communities of the Cumberland Plateau of Tennessee. *Journal of the Tennessee Academy of Science* 64(3):123–129.
- Hodges, J. A., R. J. Norell and M. H. Sarah. 2018. Tennessee. <www.britannica.com/place/Tennessee> Accessed 25 December 2020.
- Huete, A. R. 1988. A soil-adjusted vegetation index (SAVI). *Remote Sensing of Environment* 25(3):295–309.
- Jiménez, E., J. A. Vega, J. M. Fernández-Alonso, D. Vega-Nieva, L. Ortiz, P. M. López-Serrano and C. A. López-Sánchez. 2017. Estimation of aboveground forest biomass in Galicia (NW Spain) by the combined use of LiDAR, LANDSAT ETM+ and National Forest Inventory data. *iForest—Biogeosciences and Forestry* 10(3):590–596.
- Ke, Y., L. J. Quackenbush and J. Im. 2010. Synergistic use of QuickBird multispectral imagery and LiDAR data for object-based forest species classification. *Remote Sensing of Environment* 114(6):1141–1154.
- Li, W., Z. Niu, R. Shang, Y. Qin, L. Wang and H. Chen. 2020. High-resolution mapping of forest canopy height using machine learning by coupling ICESat-2 LiDAR with Sentinel-1, Sentinel-2 and Landsat-8 data. *International Journal of Applied Earth Observation and Geoinformation* 92:102163.
- Lichtenthaler, H. K., M. Lang, M. Sowinska, F. Heisel and J. A. Miehé. 1996. Detection of vegetation stress via a new high resolution fluorescence imaging system. *Journal of Plant Physiology* 148(5):599–612.
- Martinuzzi, S., W. A. Gould, O. M. Ramos Gonzalez, A. M. Robles, P. C. Maldonado, N. Pérez-Buitrago and J. J. Fumero Caban. 2008. Mapping tropical dry forest habitats integrating Landsat NDVI, Ikonos imagery, and topographic information in the Caribbean island of Mona. *Revista de Biología Tropical* 56(2):625–639.
- Mather, P. M. and M. Koch. 2011. *Computer Processing of Remotely Sensed Images: An Introduction*, 4th ed. Chichester, United Kingdom: Wiley-Blackwell.
- Matongera, T. N., O. Mutanga, T. Dube and M. Sibanda. 2017. Detection and mapping the spatial distribution of bracken fern weeds using the Landsat 8 OLI new generation sensor. *International Journal of Applied Earth Observation and Geoinformation* 57:93–103.
- Nguyen, T. 2015. Optimal ground control points for geometric correction using genetic algorithm with global accuracy. *European Journal of Remote Sensing* 48(1):101–120.
- Pehani, P., K. Čotar, A. Marsetič, J. Zaletelj and K. Oštir. 2016. Automatic geometric processing for very high resolution optical satellite data based on vector roads and orthophotos. *Remote Sensing* 8(4):343. <https://doi.org/10.3390/rs8040343>.
- Poortinga, A., K. Tenneson, A. Shapiro, Q. Nquyen, K. San Aung, F. Chishtie and D. Saah. 2019. Mapping plantations in Myanmar by fusing Landsat-8, Sentinel-2 and Sentinel-1 data along with systematic error quantification. *Remote Sensing* 11(7):831.
- Prabhakara, K., W. D. Hively and G. W. McCarty. 2015. Evaluating the relationship between biomass, percent groundcover and remote sensing indices across six winter cover crop fields in Maryland, United States. *International Journal of Applied Earth Observation and Geoinformation* 39:88–102.
- Qi, J., A. Chehbouni, A. R. Huete, Y. H. Kerr and S. Sorooshian. 1994. A modified soil adjusted vegetation index. *Remote Sensing of Environment* 48(2):119–126.
- Reid, S. L., J. L. Walker and A. Schaaf. 2016. Using multi-spectral Landsat imagery to examine forest health trends at Fort Benning, Georgia. Pages 600–603 in *Proceedings of the 18th Biennial Southern Silvicultural Research Conference*, held in Knoxville, Tennessee, March 2–5, 2015. Edited by C.J. Schweitzer, W.K.

- Rhyma, P. P., K. Norizaha, O. Hamdan, I. Faridah-Hanum and A. W. Zulfa. 2020. Integration of normalised different vegetation index and Soil-Adjusted Vegetation Index for mangrove vegetation delineation. *Remote Sensing Applications: Society and Environment* 17:100280.
- Roth, K. L., D. A. Roberts, P. E. Dennison, S. H. Peterson and M. Alonzo. 2015. The impact of spatial resolution on the classification of plant species and functional types within imaging spectrometer data. *Remote Sensing of Environment* 171:45–57.
- Rozenstein, O. and A. Karnieli. 2011. Comparison of methods for land-use classification incorporating remote sensing and GIS inputs. *Applied Geography* 31(2):533–544.
- Shang, X. and L. A. Chisholm. 2014. Classification of Australian native forest species using hyperspectral remote sensing and machine-learning classification algorithms. *IEEE Journal of Selected Topics in Applied Earth Observations and Remote Sensing* 7(6):2481–2489.
- Sharma, R. C., K. Hara and H. Hirayama. 2017. A machine learning and cross-validation approach for the discrimination of vegetation physiognomic types using satellite based multispectral and multitemporal data. *Scientifica* 2017:9086479. <https://doi.org/10.1155/2017/9806479>.
- Sinha, S., L. K. Sharma and M. S. Nathawat. 2015. Improved Land-use/Land-cover classification of semi-arid deciduous forest landscape using thermal remote sensing. *The Egyptian Journal of Remote Sensing and Space Sciences* 18(2):217–233.
- Sjöqvist, H., M. Längqvist and F. Javed. 2020. An analysis of fast learning methods for classifying forest cover types. *Applied Artificial Intelligence* 34(10):691–709.
- Skidmore, A. K., W. Bijkar, K. Schmidt and L. Kumar. 1997. Use of remote sensing and GIS for sustainable land management. *ITC Journal*, 3/4:302–315.
- Starnes, D. D. 1986. *Tennessee Topology*. Location: Tennessee Department of Environment and Conservation.
- Tawfeik, M., H. Elhifnawy, E. Hamza and A. Shawky. 2016. Determination of suitable requirements for geometric correction of remote sensing satellite images when using ground control points. *International Research Journal of Engineering and Technology* 3(10):54–62.
- Twele, A., W. Cao, S. Plank and S. Martinis. 2016. Sentinel-1-based flood mapping: A fully automated processing chain. *International Journal of Remote Sensing* 37(13):2990–3004.
- United States Department of Agriculture. 2021. Fire Effects Information System (FEIS) Index of Species Information. <https://www.fs.fed.us/database/feis/plants/tree/pinech/all.html> Accessed 12 May 2021.
- United States Geological Survey. 2019. *Landsat 8 (L8) Data Users Handbook*, version 5.0. Location: United States Geological Society.
- van Aardt, J.A.N. and R. H. Wynne. 2007. Examining pine spectral separability using hyperspectral data from an airborne sensor: Extension of field-based results. *International Journal of Remote Sensing* 28(2):431–436.
- van Ewijk, K. Y., C. F. Randin, P. M. Treitz and N. A. Scott. 2014. Predicting fine-scale tree species abundance patterns using biotic variables derived from LiDAR and high spatial resolution imagery. *Remote Sensing of Environment* 150:120–131.
- Vincent, S., S.A.J. Francis, K. Raimond and O. P. Kumar. 2019. A study of types of sensors used in remote sensing. *International Journal of Electronics and Telecommunications* 65(2):217–228.
- Wan, H., Y. Tang, L. Jing, H. Li, F. Qiu and W. Wu. 2021. Tree species classification of forest stands using multisource remote sensing data. *Remote Sensing* 13(1):144.
- Xie, Y., Z. Sha and M. Yu. 2008. Remote sensing imagery in vegetation mapping: A review. *Journal of Plant Ecology* 1(1):9–23.
- Xu, H. 2006. Modification of normalised difference water index (NDWI) to enhance open water features in remotely sensed imagery. *International Journal of Remote Sensing* 27(14):3025–3033.
- Xue, J. and B. Su. 2017. Significant remote sensing vegetation indices: A review of developments and applications. *Journal of Sensors* 2017:1353691.
- Young, T. M., D. G. Hodges and T. G. Rials. 2007. The forest products economy of Tennessee. *Forest Products Journal* 57(4):12–19.